CRISPR

Type III-B CRISPR-Cas cascade of proteolytic cleavages

Jurre A. Steens[1,2]†, Jack P. K. Bravo[3]†, Carl Raymund P. Salazar[1]†, Caglar Yildiz[1], Afonso M. Amieiro[1], Stephan Köstlbacher[1], Stijn H. P. Prinsen[2], Ane S. Andres[1], Constantinos Patinios[1], Andreas Bardis[1], Arjan Barendregt[4], Richard A. Scheltema[4], Thijs J. G. Ettema[1], John van der Oost[1], David W. Taylor[3], Raymond H. J. Staals[1]*

The generation of cyclic oligoadenylates and subsequent allosteric activation of proteins that carry sensory domains is a distinctive feature of type III CRISPR-Cas systems. In this work, we characterize a set of associated genes of a type III-B system from *Haliangium ochraceum* that contains two caspase-like proteases, SAVED-CHAT and PCaspase (prokaryotic caspase), co-opted from a cyclic oligonucleotide–based antiphage signaling system (CBASS). Cyclic tri–adenosine monophosphate (AMP)–induced oligomerization of SAVED-CHAT activates proteolytic activity of the CHAT domains, which specifically cleave and activate PCaspase. Subsequently, activated PCaspase cleaves a multitude of proteins, which results in a strong interference phenotype in vivo in *Escherichia coli*. Taken together, our findings reveal how a CRISPR-Cas–based detection of a target RNA triggers a cascade of caspase-associated proteolytic activities.

Type III CRISPR-Cas systems are adaptive immune systems in prokaryotes that use CRISPR-derived RNA (crRNA) guides to target the complementary RNA of invading viruses and plasmids. Type III systems have many distinctive features, including a rapidly expanding network of signal transduction pathways to trigger dormancy or cell death (*1*–*3*).

A typical type III operon encodes multiple Cas proteins that form a type III effector complex with a mature crRNA. These complexes bind complementary target RNAs, a process that is initiated at an exposed seed region at the 3′ end of the crRNA. Seed-binding licenses complete base pairing between the target RNA and the crRNA, thereby activating Cas10, the signature multidomain subunit of the type III complex (*4*). The histidine-aspartate (HD) nuclease domain of activated Cas10 degrades single-stranded DNA substrates in a non–sequence-specific manner, whereas the Palm domain acts as a cyclase to convert adenosine triphosphate (ATP) into signaling molecules called cyclic oligoadenylates (cOAs), that is, rings of three to six adenosine monophosphate (AMP) moieties (*5*–*9*). These cOAs activate a set of effector proteins that carry a cOA-binding domain, either CARF or SAVED (*8*–*10*). These sensory domains are generally fused to catalytic domains [e.g., ribonucleases (RNases), deoxyribonucleases (DNases), nicotinamide adenine dinucleotide nucleosidases (NADases), and toxins], which leads to diverse activities (*11*–*13*). Over the past few years, a handful of these CARF and SAVED proteins have been characterized, revealing various activities geared toward killing the host or inducing dormancy, which stops the spread of the invading nucleic acid (e.g., phage progeny, plasmid propagation, etc.) in a process known as abortive infection. Recent work on type III systems has indicated that proteases also play a role in type III immunity, particularly TPR-CHAT (Csx29), which physically associates with the type III-E complex, and a cOA-activated Lon-like protease (CalpL) in a type III-B system (*14*, *15*).

Results

Type III-B CRISPR-Cas–CBASS hybrid

We identified a set of genes flanking an operon that encodes a type III-B CRISPR-Cas protein complex (*Cmr1* to *Cmr6*) in *Haliangium ochraceum* DSM 14365 (Fig. 1A). We observed a *SAVED-CHAT* gene, which encodes a fusion protein of a SAVED domain and a CHAT domain (related to cysteine proteases that include caspases, which are involved in programmed cell death in eukaryotes) (Fig. 1B). Further downstream, we observed a gene encoding a caspase-like cysteine protease (annotated as "peptidase C14 caspase catalytic subunit p20"), which we named *PCaspase* (prokaryotic caspase) (Fig. 1C). Located in between these genes are three genes that encode (i) a predicted sigma factor we named *PC*-σ (prokaryotic caspase sigma factor); (ii) a hypothetical protein we named *PCi* (prokaryotic caspase inhibitor), owing to predicted structural homology with the CI-2 family of serine protease inhibitors; and (iii) a serine-threonine protein kinase we named *PCk* (prokaryotic caspase kinase). A similar operon appears to be located elsewhere on the chromosome of *H. ochraceum* (fig. S1A).

We explored the co-occurrence of these genes in other prokaryotic genomes. We identified six additional bacterial genomes that encode *SAVED-CHAT* and *PCaspase* genes within the same gene cluster from the phyla Myxococcota (n = 2), Bacteriodota (n = 2), and Cyanobacteria (n = 1) (Fig. 1D). Only the gene cluster of *Enhygromyxa salina_A* contained a gene set comparable to that of *H. ochraceum*, excluding *PCi*, for which homologs could not be identified in other prokaryotes. Two of the operons encoded type III CRISPR-Cas systems in the neighboring regions, whereas the remaining four operons encoded cGAS/DncV-like nucleotidyltransferase (CD-NTase) domains, indicative of cyclic oligonucleotide–based antiphage signaling systems (CBASS) (*16*, *17*).

Sensory domains like SAVED are often fused to different types of effector domains, which implies a separate evolutionary origin of the two domains in *SAVED-CHAT* (Fig. 1, B and E). Phylogenetic analysis showed that the CHAT domains of the two *H. ochraceum SAVED-CHAT* variants were only distantly related, indicating independent acquisition events (fig. S1B). The SAVED domains, however, formed a monophyletic clade (Fig. 1E) and were likely acquired once and duplicated into two *SAVED* copies, to which CHAT domains of different origin were subsequently added. This scenario is further supported by phylogenies of *PCaspase*, *PC*-σ, and *PCk* (fig. S1, C to E), which all support monophyly of the two respective copies. The SAVED domains are most closely related to those of other Myxococcota and might be part of a conserved system in these bacteria. All but one gene neighborhood of *SAVED-CHAT* relatives contained a setup reminiscent of a CBASS defense system (Fig. 1F), with two or three putative cyclases, a protein kinase homolog of *PCk*, a *sigma-70*–like sigma factor, and a ubiquitin-activating *thiF* gene. Taken together, these findings suggest that cOA sensory and effector components of a CBASS system were co-opted in *H. ochraceum* to work in tandem with a type III CRISPR-Cas system. The pairing of a type III CRISPR-Cas "signal generator" with a CBASS effector is reminiscent of NucC [a cyclic tri-AMP (cA_3)–activated, promiscuous nuclease] that has been described previously (*18*, *19*).

SAVED-CHAT and PCaspase cleavage activity

We anticipated that SAVED-CHAT acts as a cOA-activated protease with a selective substrate repertoire similar to that of other CHAT cysteine proteases (*20*). To test this hypothesis, we purified all type III–associated proteins from *H. ochraceum*, excluding PCk, which could not be cloned individually or in combination with PC-σ and PCi, likely because of toxicity. We investigated SAVED-CHAT substrate specificity using in vitro cleavage assays with the other three proteins and observed that SAVED-CHAT specifically cleaves PCaspase in a cA_3-dependent and cofactor-independent manner (Fig. 2A and figs. S2 and S3), but not PC-σ and PCi (Fig. 2B).

[1]Laboratory of Microbiology, Wageningen University and Research, Wageningen, Netherlands. [2]Scope Biosciences B.V., Wageningen, Netherlands. [3]Department of Molecular Biosciences, University of Texas at Austin, Austin, TX, USA. [4]Biomolecular Mass Spectrometry and Proteomics, University of Utrecht, Utrecht, Netherlands.
*Corresponding author. Email: raymond.staals@wur.nl
†These authors contributed equally to this work.

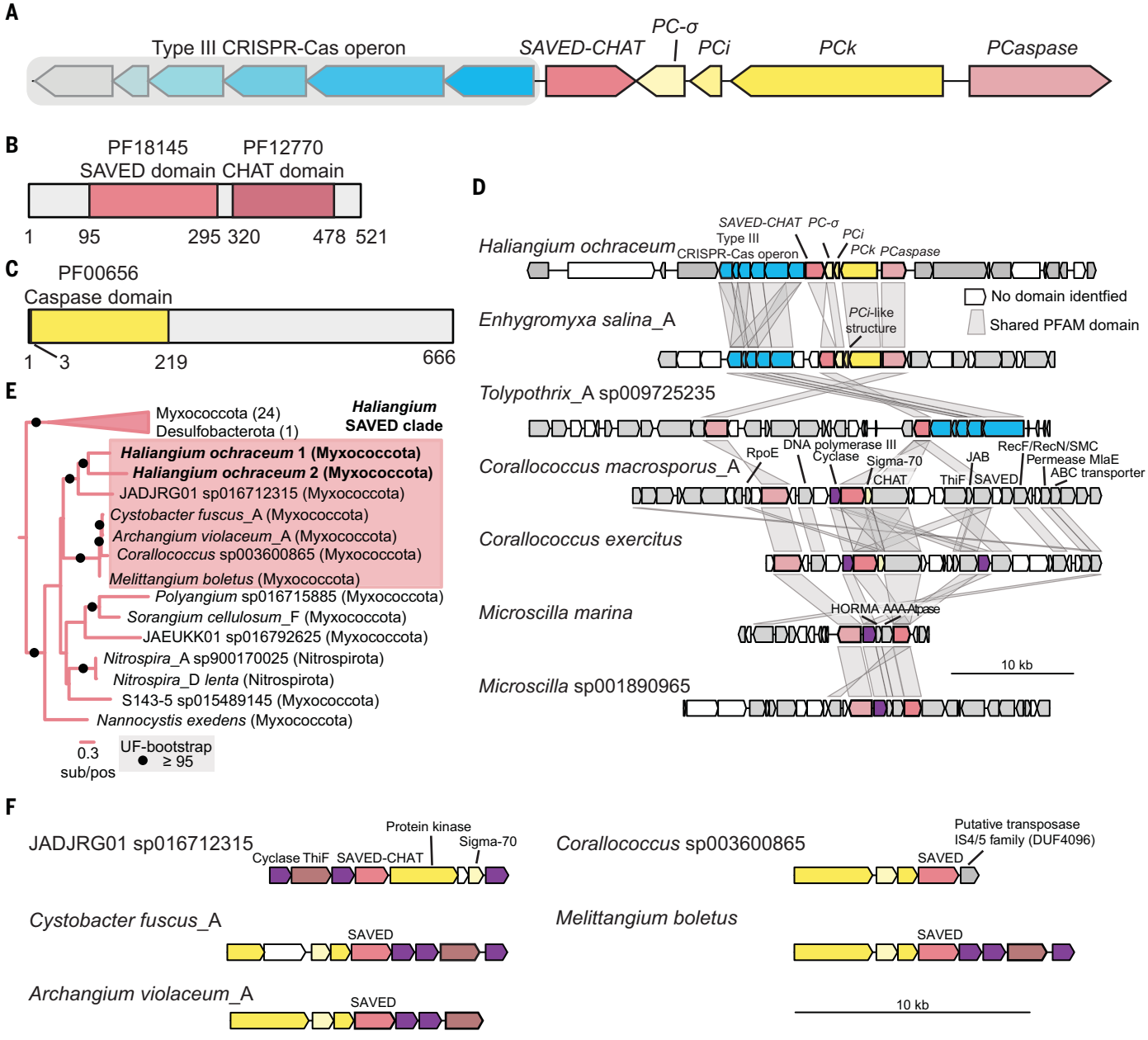

Fig. 1. Type III CRISPR-Cas operon–associated *SAVED-CHAT–PCaspase* gene cluster setup and CBASS origin. (**A**) Schematic representation of the *H. ochraceum* type III-B CRISPR-Cas operon that contains (i) the *Cmr1* to *Cmr6* genes that encode the crRNA-guided type III protein complex and (ii) the complex's associated genes: *SAVED-CHAT*, *PC-σ*, *PCi*, *PCk*, and *PCaspase* (locus tags Hoch_1313 to Hoch_1323). (**B**) Domain architecture of SAVED-CHAT. (**C**) Domain architecture of PCaspase. (**D**) Genomic neighborhoods containing *SAVED-CHAT* and *PCaspase*. (**E**) SAVED domain phylogenetic midpoint-rooted tree. (**F**) CBASS-type operons containing *Haliangium* SAVED clade domains with associated proteins that contain cyclase, protein kinase, sigma-70, and transposase domains.

SAVED-CHAT cleaved PCaspase into several defined fragments in addition to a myriad of products. A catalytically dead version of SAVED-CHAT [dSAVED-CHAT, which contains substitutions H375A (His^{375}→Ala) and C422A (Cys^{422}→Ala)] showed no activity (fig. S2). Furthermore, we noticed that the addition of cA_3 prevented the migration of SAVED-CHAT in native polyacrylamide gel electrophoresis (PAGE), which indicates that SAVED-CHAT oligomerizes to form large complexes in the presence of cA_3 (fig. S4).

To elucidate how PCaspase is activated upon cleavage by SAVED-CHAT, we used AlphaFold2 (AF2) to predict the structure of PCaspase. The H79-C146 catalytic dyad of PCaspase was obstructed by an unstructured loop (residues 144 to 163) (fig. S5, A and B), which suggests a mechanism whereby PCaspase is autoinhibited.

Because the protease active site of SAVED-CHAT lies within a narrow channel, we hypothesized that the PCaspase cleavage site would reside within an unstructured loop. To identify a putative PCaspase cleavage site, we used AF2 multimer to cofold the CHAT domain of SAVED-CHAT with ~10- to 20-residue-long unstructured peptides of PCaspase. We found that the peptide that obstructs the PCaspase catalytic dyad was predicted to form an interaction with SAVED-CHAT, with a single arginine residue at position 153 (R153) predicted to fit into the active site with a high confidence score (89.3) (fig. S5C). An AF2 model of the processed PCaspase fragment residues 1 to 153 appears to be catalytically competent. Indeed, activated SAVED-CHAT was unable to

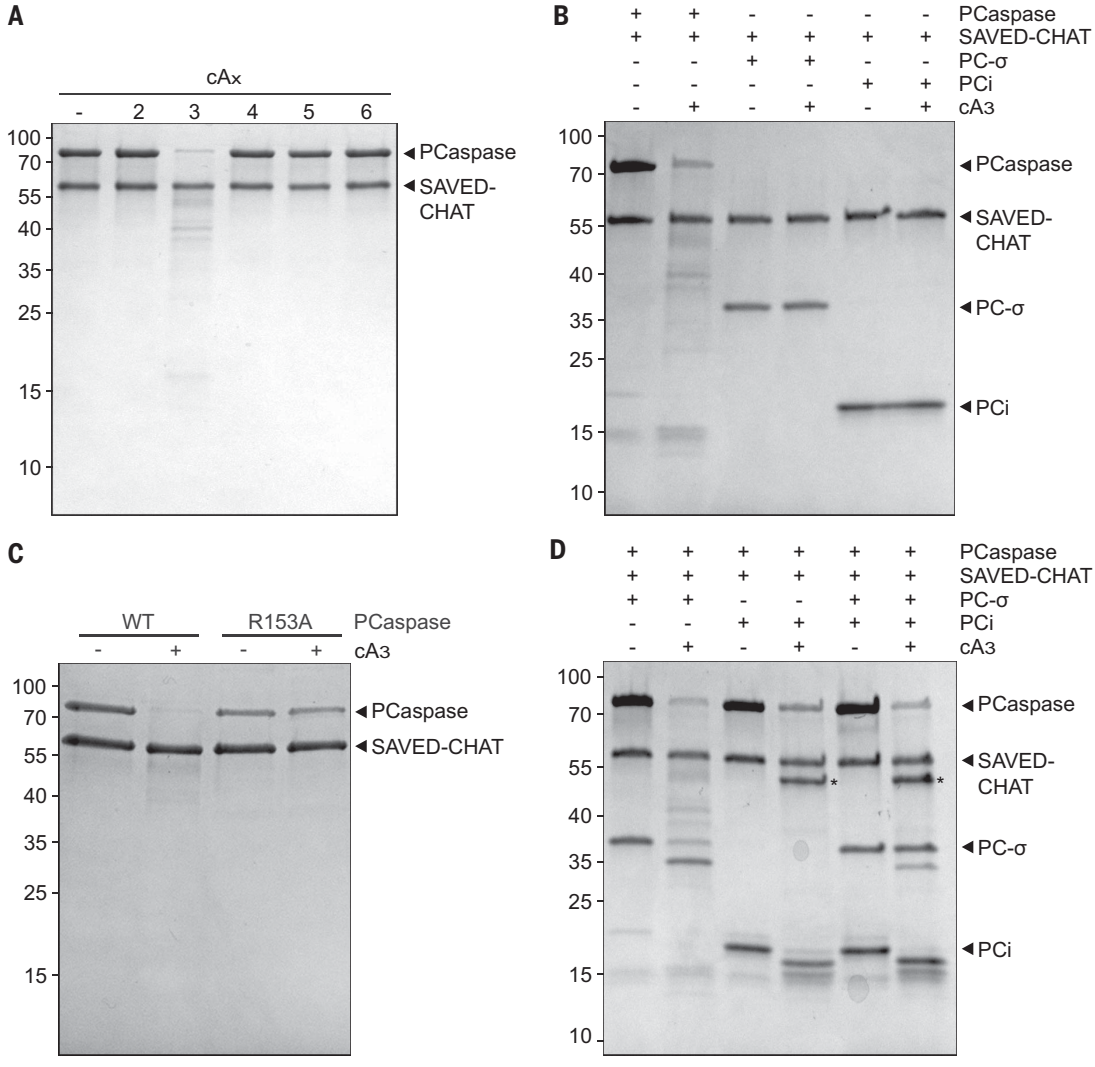

Fig. 2. cA_3-induced SAVED-CHAT and subsequent PCaspase activity. (**A**) SDS-PAGE analysis of SAVED-CHAT cleavage, which shows its dependency on cA_3 for cleaving PCaspase. (**B**) SDS-PAGE analysis of cleavage activity of activated SAVED-CHAT on PC-σ and PCi. (**C**) SDS-PAGE analysis of SAVED-CHAT cleavage on wild-type (WT) PCaspase and the R153A PCaspase mutant. (**D**) SDS-PAGE analysis of cleavage activity of activated PCaspase on PC-σ and PCi. Activated PCaspase cleaves PC-σ and PCi individually; PC-σ is cleaved less when PCi is present. The stabilized PCaspase fragment is indicated with an asterisk.

cleave an R153A (Arg^{153}→Ala) PCaspase mutant, which shows that R153 is essential for cleavage (Fig. 2C). Shotgun and top-down proteomic profiling of cleaved PCaspase fragments confirmed cleavage at R153 (fig. S6). Notably, R153 was highly conserved in other PCaspase homologs that co-occurred with SAVED-CHAT (fig. S7A). The AF2 model predicted that PCaspase R153 would interact with SAVED-CHAT asparagine residue N420 and glutamic acid residue E328 (fig. S5F), which were fully conserved or conserved as pairs in several homologs with a co-occurring PCaspase (fig. S7B).

Next, we performed protein cleavage assays with SAVED-CHAT and PCaspase using different combinations of PC-σ and PCi (Fig. 2D). PCaspase cleavage by activated SAVED-CHAT resulted in the subsequent cleavage of PC-σ and PCi into defined cleavage products. These results indicate that PCaspase cleavage by SAVED-CHAT activates its proteolytic activity. When PCi was present, one of the cleaved PCaspase fragments was stabilized and other degradation products of PCaspase were absent, which hints at self-degradation (Fig. 2D). Furthermore, PCi decreased the efficiency of PCaspase-mediated PC-σ cleavage in a concentration-dependent manner, indicating that PCi acts as an inhibitor for PCaspase activity (Fig. 2D and fig. S8).

PCaspase-mediated cleavage of PC-σ and PCi prompted us to hypothesize that PCaspase might have a broad substrate repertoire. Indeed, activated PCaspase was able to degrade a biologically unrelated casein, whereas SAVED-CHAT by itself did not (Fig. 3A and fig. S9). Other unrelated proteins were also degraded by activated PCaspase but not activated by SAVED-CHAT, which further demonstrates the broad range of PCaspase substrates (fig. S10). Furthermore, a catalytically dead mutant of PCaspase [dPCaspase, which contains substitutions H79A (His^{79}→Ala) and (Cys^{146}→Ala)] showed no activity (Fig. 3A). PCi also inhibited PCaspase-mediated casein degradation in a concentration-dependent manner, which indicates that the PCi inhibitory effect is independent of PC-σ (fig. S11).

The broad substrate repertoire of PCaspase allowed us to monitor its activity in real time by providing a small fluorophore-quencher peptide as a substrate (Fig. 3B and fig. S12). We showed an inverse relationship between PCaspase reaction kinetics and PCi concentration (Fig. 3C). We probed the sensitivity and kinetics of this detection method to cA_3 and achieved near-instant signal generation in the presence of >31.2 nM of cA_3, with a limit of detection of 15.6 nM (Fig. 3D). Lastly, we elucidated the target residue of activated PCaspase by testing six different fluorophore-quencher peptides that contained different combinations of candidate residues typically targeted by caspase-like cysteine proteases (*21*). All cleaved peptides contained an arginine (Fig. 3E), which suggests that activated PCaspase cleaves at arginines in unstructured peptides.

SAVED-CHAT and PCaspase activation leads to a strong defense mechanism phenotype

Owing to the apparent broad substrate specificity of PCaspase, we hypothesized that the sequential activation of *H. ochraceum* type III CRISPR-Cas by a target RNA, SAVED-CHAT,

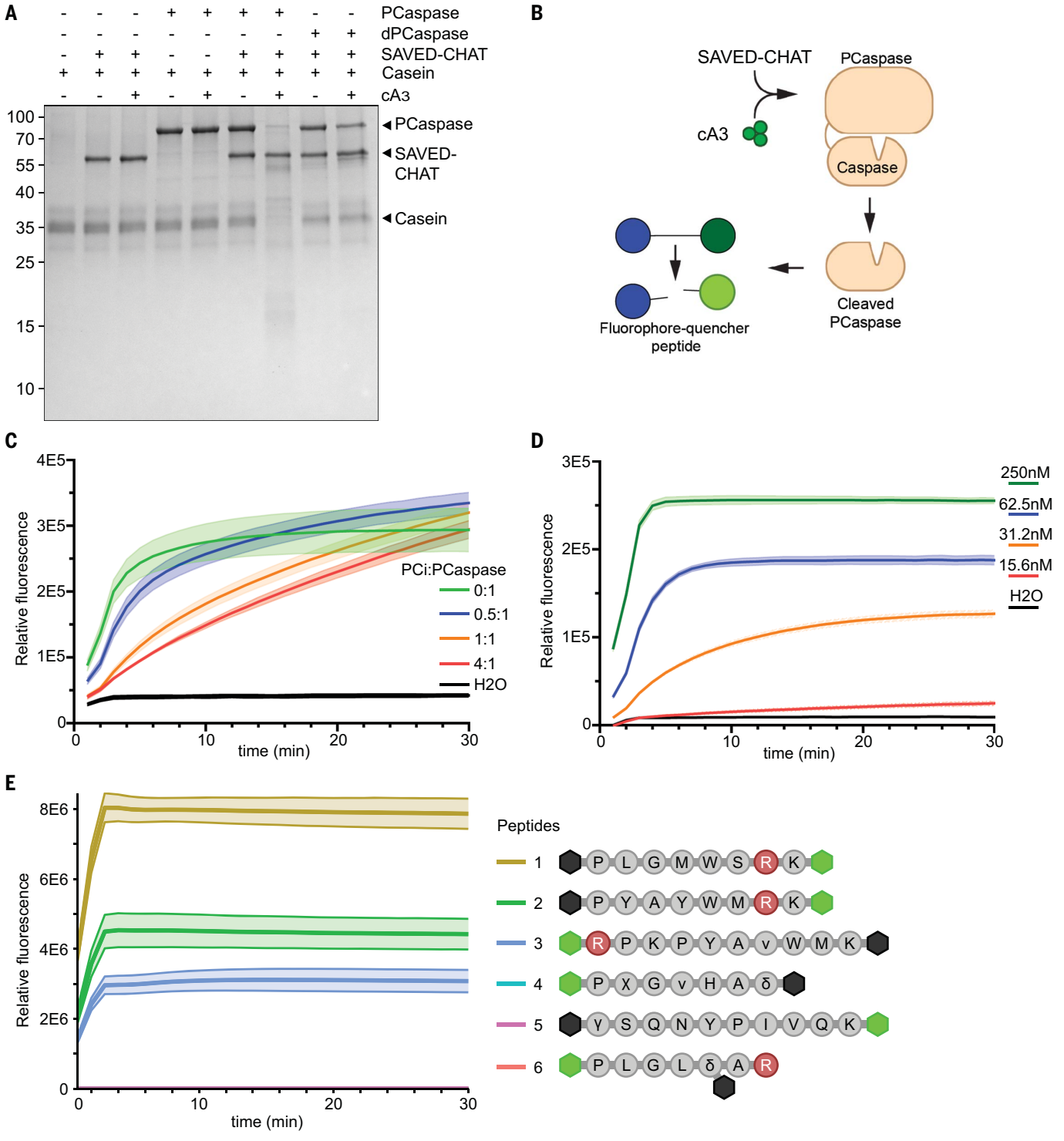

Fig. 3. PCaspase activity on nonassociated substrates. (**A**) SDS-PAGE analysis of the proteolytic activation of PCaspase by SAVED-CHAT, which results in degradation of the casein substrate, in contrast to activated SAVED-CHAT by itself or the dPCaspase catalytic mutant (H79A, C146A). (**B**) Schematic overview of PCaspase activity assay using a fluorescent peptide reporter. (**C**) Increasing the molar ratio (PCi:PCaspase) of PCi reduces the cleavage activity of a carboxy-fluorescein (FAM)–peptide substrate by activated PCaspase. The shaded regions represent the standard error of the mean (n = 3 technical replicates). (**D**) Sensitivity for cA_3 of the FAM-peptide visualization method is 15.6 nM. The shaded regions represent the standard error of the mean (n = 3 technical replicates). (**E**) PCaspase cleaves reporter peptides that contain arginines. Arginines are in red, fluorophores are in green, and quenchers are in black. Shaded regions represent the standard error of the mean (n = 3 technical replicates). ν, norvaline; χ, cyclohexylalanine; δ, diaminobutyric acid; γ, GABA. Single-letter abbreviations for the amino acid residues are as follows: A, Ala; G, Gly; H, His; I, Ile; K, Lys; L, Leu; M, Met; N, Asn; P, Pro; Q, Gln; R, Arg; S, Ser; V, Val; W, Trp; and Y, Tyr.

and eventually PCaspase could affect cell viability. We therefore constructed the pHochTypeIII plasmid, which encodes *H. ochraceum Cmr1* to *Cmr6* (forming the type III complex), *csb2* (a *cas6* homolog that processes the pre-crRNA), and a minimal CRISPR array that contains two repeats and a spacer (fig. S13A) (*22*). The SAVED-CHAT and PCaspase genes were expressed in different combinations from the pEffector plasmid (fig. S13B). NucC (a cA_3-responsive nuclease that causes abortive infection) from *Escherichia coli* MS115-1 and an empty vector were used as positive and negative controls, respectively (fig. S13B) (*23*). Target and nontarget plasmids encoded an isopropyl-β-D-thiogalactopyranoside (IPTG)–inducible protospacer that was complementary and noncomplementary to the spacer, respectively (fig. S13C) (*24*).

The target or nontarget plasmid was transformed into *E. coli* BL21-AI that harbored pHochTypeIII and one of the pEffector plasmids (Fig. 4A). Ten-fold serial dilutions were plated on glucose- or IPTG-containing plates to repress or induce, respectively, the target or nontarget RNA to calculate transformation efficiencies. First, we demonstrated that the *H. ochraceum* type III system produces cA_3 upon target RNA recognition and leads to an abortive infection phenotype in the presence of NucC (Fig. 4B) (*23*). When both SAVED-CHAT and PCaspase were present, target RNA expression reduced transformation efficiency by six orders of magnitude (Fig. 4B and fig. S13D). Additionally, we investigated the in vivo effect of expressing different combinations of the two expected PCaspase fragments after R153 cleavage, along with SAVED-CHAT. None yielded a strong reduction in transformation efficiency compared with expression of full-length, wild-type PCaspase, perhaps owing to changes in the structural conformations of the fragments or weaker interactions when they were expressed separately (fig. S14). Overall, we confirmed that *H. ochraceum* type III-B produces (at least) cA_3 and mounts a robust defense response in combination with its effector proteins SAVED-CHAT and PCaspase.

To investigate the inhibitory effect of PCi on PCaspase in vivo, we cloned it with and without PC-σ into the pSAVED-CHAT_PCaspase plasmid (fig. S13B). The results showed that upon target RNA expression, PCi improved transformation efficiency by two orders of magnitude (irrespective of the presence of PC-σ) compared with SAVED-CHAT and PCaspase alone (Fig. 4C and fig. S13E). This is in agreement with the observed in vitro PCi-mediated PCaspase inhibition and shows that in vivo, PCi alleviates the PCaspase-mediated defense mechanism phenotype. Unfortunately, we were unable to produce a strain that expressed PC-σ in combination with SAVED-CHAT and PCaspase, likely because of toxicity.

Structural basis for SAVED-CHAT activation

To understand the structural basis for cA_3-induced activation of SAVED-CHAT, we determined a cryo–electron microscopy (cryo-EM) structure of the activated SAVED-CHAT in complex with cA_3. Size-exclusion chromatography and negative staining indicated that SAVED-CHAT is monomeric in solution, whereas cA_3 binding induced the formation of large, polydisperse oligomers, as observed with native PAGE (figs. S4, S15, and S19). Prolonged incubation of cA_3 with SAVED-CHAT resulted in the formation of large, polymorphous aggregates that were not amenable to structural determination (fig. S16A). However, by vitrifying immediately after

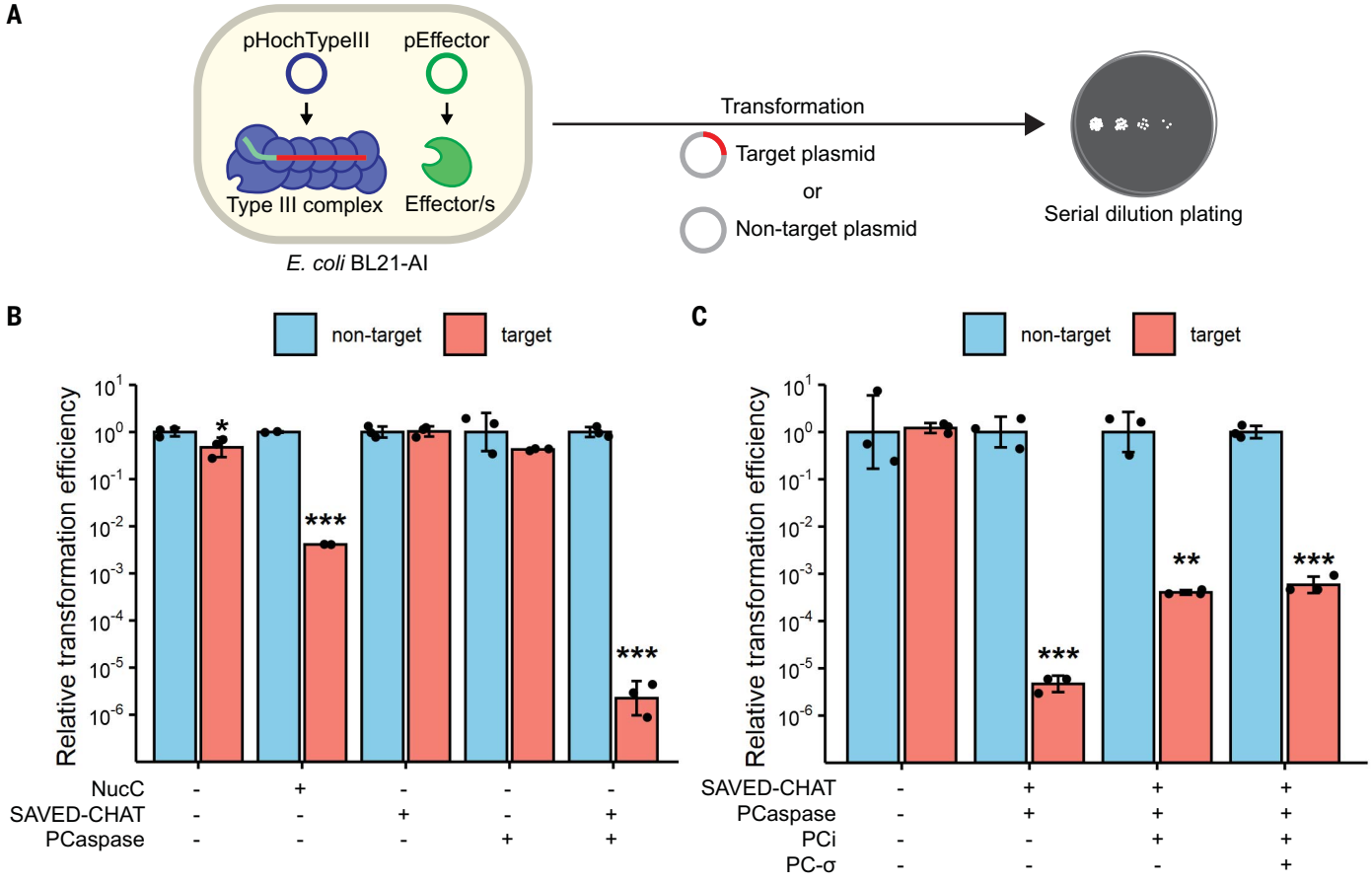

Fig. 4. PCaspase activation reduces the transformation efficiency of a target plasmid. (**A**) Schematic overview of the experimental setup in *E. coli* BL21-AI. (**B**) Transformation efficiencies (relative to the nontarget control) of target or nontarget plasmid in *E. coli* coexpressing *H. ochraceum* type III CRISPR-Cas complex and different combinations of effector proteins. (**C**) Transformation efficiencies (relative to the nontarget control) when SAVED-CHAT and PCaspase are coexpressed with PCi and PC-σ. Error bars represent the standard deviation of the mean. Statistical significance was calculated using one-sided unpaired Welch's *t* test (n = 3 biological replicates). *p < 0.05; **p < 0.005; ***p < 0.0005.

mixing SAVED-CHAT and cA_3, we were able to obtain a structure of the filament at a global resolution of 3.1 Å (figs. S16, B to H, and S17 and table S1).

SAVED-CHAT oligomerization results in long, curved filaments with the SAVED domain on the inside and the CHAT domains at the periphery, with a curvature of ~10° between each monomer (Fig. 5A and fig. S16). SAVED-CHAT monomers assemble through head-to-tail oligomerization, with a single cA_3 bound at the interface between two SAVED domains, forming "singlet" filaments. We additionally observed partial "doublets" in which two antiparallel filaments make a cross-fiber interaction that spans up to three SAVED-CHAT monomers (Fig. 5A).

In the singlet regions of our map, the CHAT domains were poorly resolved and often absent, which was likely due to conformational flexibility (Fig. 5, B and C). Analysis of AF2 models of monomeric SAVED-CHAT revealed a high degree of flexibility between the two globular domains, with an unstructured linker (residues 297 to 304) acting as a hinge to accommodate a maximum displacement of up to 35 Å (fig. S18A). It is likely that the strain induced by the filament curvature prevents more than three successive CHAT domains from forming stable interfiber contacts.

The intrafilament head-to-tail CHAT-CHAT interface is composed of a four-helix bundle,

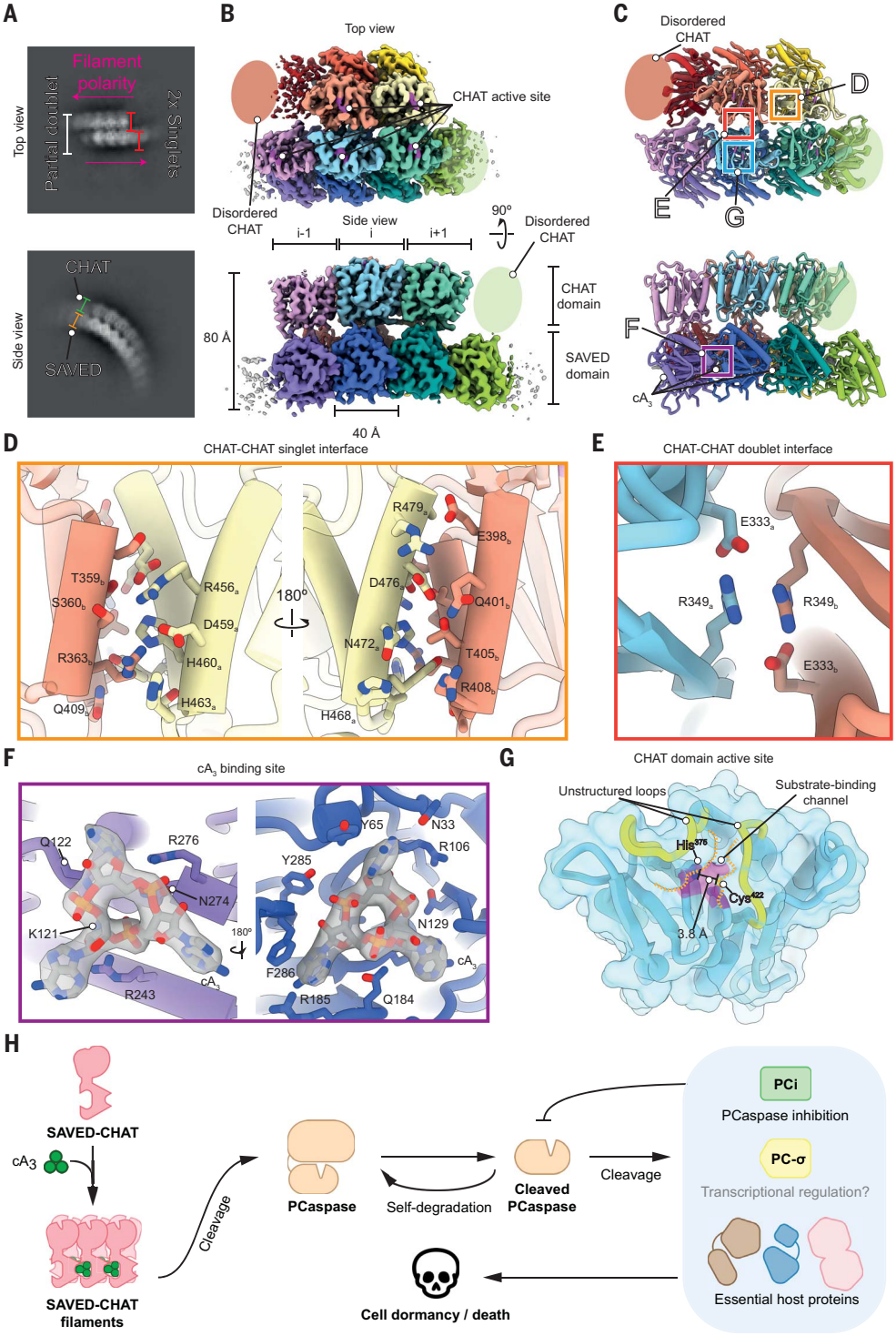

Fig. 5. Structural basis for SAVED-CHAT activation by cA_3. (**A**) Representative two-dimensional class averages of SAVED-CHAT bound to cA_3, showing side and top views. In the side view, the filament curvature is evident, with the CHAT domain at the periphery of the arch. In the top view, singlet filaments form a partial interfilament doublet, with two singlets running in opposite polarities, forming cross-fiber contacts that span ~3 monomers. (**B** and **C**) 3.1-Å–resolution cryo-EM reconstruction (B) and model (C) of the cA_3-bound SAVED-CHAT filament. In some monomers, the CHAT domain is disordered and absent from the reconstruction (red and light green monomers). In (C), the rectangles highlight areas that are magnified in (D) to (G). (**D**) Close-up view of the CHAT-CHAT singlet intrafilament interface, which consists of a four-helix bundle. T, Thr. (**E**) Close-up view of the CHAT-CHAT doublet inter filament interface. (**F**) cA_3 binding site, at the interface between adjacent SAVED domains. The cryo-EM density for cA_3 is shown as translucent gray. F, Phe. (**G**) CHAT domain active site. Residues H375 and C422 that make up the catalytic dyad (magenta) are 3.8 Å apart and located within the substrate-binding channel beneath two unstructured gating loops (yellow). (**H**) Binding of cA_3 to the SAVED domain of SAVED-CHAT induces oligomerization that activates its CHAT domain. Activated SAVED-CHAT cleaves PCaspase, which subsequently mediates further downstream events by cleaving PCi (inhibitor of PCaspase), PC-σ (transcriptional response?), and/or other essential host proteins. Hypothesized events are in gray.

with two helices from each protomer (Fig. 5D). This bundle is held together through a network of predominantly electrostatic interactions, which is consistent with a SAVED-CHAT mutant in which this interface was perturbed (fig. S19). The CHAT-CHAT interfilament doublet interface is mediated by an unusual π-π stacking interaction between two R349 residues (the same residue from different monomers), reinforced by additional electrostatic contacts (Fig. 5E).

The cA_3 is buried within the intrafilament interface between two SAVED domains and participates extensively in hydrogen bonding and electrostatic and stacking interactions, similar to its role in other SAVED domains (Fig. 5F and fig. S20). This network of contacts suggests that cA_3 acts as a molecular glue to bridge SAVED domain intrafilament interactions (fig. S19), which subsequently provides a platform for CHAT-CHAT interdomain interactions that allosterically activate protease activity. This is a distinct mechanism of activation from that of the TIR-SAVED filaments, which assemble a composite active site across two adjacent TIR domains within a filament upon cA_3 binding, or the CRISPR-associated Lon protease (CalpL) activation that appears to have a concentration-dependent effect, which reflects the mechanistic diversity of cOA-responsive effector proteins (*15*, *25*).

Within the resolved doublet CHAT domains, the active site is positioned underneath two unstructured loops, which creates a narrow substrate-binding channel (Fig. 5G). This channel is wide enough to accommodate unstructured peptides but would likely be inaccessible to highly structured peptides. The residues of the H375-C422 catalytic dyad are aligned and positioned ~4 Å apart, confirming that the cA_3-bound filament represents the active conformation of SAVED-CHAT. Comparison with the CHAT domain of the activated type III-E protein TPR-CHAT bound to proteolytic substrate Csx30 revealed a near identical active-site configuration in which the catalytic dyad is aligned and the substrate-binding channel is exposed (fig. S18B). We propose that SAVED-CHAT activation may occur through a conformational change in the CHAT active site, where autoinhibition is allosterically alleviated through interdomain CHAT-CHAT contacts that occur after cA_3-induced oligomerization. This is consistent with the well-established activation mechanisms of eukaryotic caspases, which are inhibited as monomers and become allosterically activated upon dimerization (*26*).

Discussion

Caspases are a family of cysteine proteases that generally use a catalytic cysteine residue to target proteins by cleaving a peptide bond. Caspases in animals typically cut after an aspartate, whereas caspases in fungi and plants (metacaspases) cut after arginine or lysine (*27*–*32*). In eukaryotes, caspases are key players in signal transduction pathways that often trigger programmed cell death (apoptosis) (*30*, *33*). These apoptotic pathways consist of two classes of caspases: initiators and executioners, with the former proteolytically activating the latter to trigger further downstream events (*26*). Our work highlights a conceptual similarity on this theme in prokaryotes: a cOA-sensory SAVED domain that activates a caspase-like CHAT domain (analogous to an initiator), which in turn activates a second caspase-like protease PCaspase (analogous to an executioner) that acts as the central node, causing a cascade of events. PCaspase appears to modify downstream targets that promote dormancy and/or cell death in vivo.

The model in Fig. 5H summarizes our present understanding of the *H. ochraceum* type III-B CRISPR-Cas system and its effector components, in which detection of target RNA results in cA_3 generation (not shown in the schematic) (*8*, *9*). The synthesized cA_3 binds to the sensory domain of SAVED-CHAT and acts as a molecular glue to stabilize SAVED:SAVED dimerization (Fig. 5). The subsequent multimerization of the unusual antiparallel SAVED-CHAT doublet filament allosterically activates the CHAT domains, an unprecedented mechanism for CARF and SAVED effector proteins (Fig. 5). The activated CHAT domains in turn cleave PCaspase, which becomes an active, promiscuous protease that cleaves a wide range of substrates. In contrast to the substrate specificity of SAVED-CHAT, PCaspase has a broader substrate repertoire, as reflected by the cleavage of PC-σ, PCi, and other unrelated proteins and fluorophore-quencher peptides in vitro (Figs. 2D and 3 and fig. S10). This is further supported by the strong abortive infection–like phenotype that is observed when PCaspase is activated in vivo (Fig. 4), where cleavage of host factors most likely leads to the significantly reduced transformation efficiency.

We found that PCi is a potent inhibitor of PCaspase both in vitro and in vivo, which hints at an autoregulated feedback loop that specifically controls PCaspase activity (Fig. 2). Furthermore, the predicted sigma factor PC-σ might be involved in coordinating additional defense strategies through transcriptional regulation (Fig. 5H), as has been suggested for CASP-σ in type III-E systems (*34*). In that study, it was shown that CASP-σ is part of a subcomplex together with Csx30 (a hypothesized toxin) and Csx31, which both lack any similarity to either PCi or PCk (fig. S21). Upon target RNA binding by the type III-E complex, the associated protease TPR-CHAT cleaves Csx30 and releases CASP-σ for transcriptional regulation of target genes that may include Cas1, which hints at a connection between interference and spacer adaptation. Another recent work on a type III-B system showed that CalpL (a Lon-like protease fused to a SAVED domain) forms a complex with CalpT (a potential anti–sigma factor) and CalpS (a sigma factor) (*15*). Upon cOA signaling, CalpL oligomerizes and subsequently cleaves CalpT, releasing a subcomplex consisting of a CalpT fragment and CalpS that is thought to regulate gene expression by RNA polymerase.

Probably owing to toxicity, all attempts to (co)purify PCk or include it in the in vivo experiments failed. We hypothesize that activated PCaspase might proteolytically modify and activate PCk, thereby activating another signal transduction pathway. Bacterial serine-threonine kinases act in stress response and antiphage defense by phosphorylating several target proteins and, in some cases, hampering growth (*35*, *36*). Hence, it might be that the anticipated cytotoxicity of PCk reflects its serine-threonine kinase activity, which may instigate abortive infection, either directly in response to a PCaspase-mediated cleavage or indirectly through transcriptional activation by PC-σ. Another remaining question is how PCaspase activity is suppressed by PCi. We speculate that this negative-feedback mechanism may allow for down-regulating the stress response to a reversible dormancy state rather than going irreversibly to cell death.

In recent years, an unprecedented diversity of type III CRISPR-Cas cOA-based signal transduction pathways have been described, but many details remain to be uncovered (*1*, *2*). Most notably, the full impact of further downstream events after activation of CRISPR-associated proteases is not fully understood and is very likely to vary between different CRISPR-Cas systems. The variant described in this work is an intriguing example of evolutionary tinkering of prokaryotic immune systems that transduces stress signals through a set of caspase-like proteases to trigger a strong defense response.

REFERENCES AND NOTES

1. S. P. B. van Beljouw, J. Sanders, A. Rodríguez-Molina, S. J. J. Brouns, *Nat. Rev. Microbiol.* **21**, 21–34 (2023).
2. J. A. Steens, C. R. P. Salazar, R. H. J. Staals, *Biochem. Soc. Trans.* **50**, 1353–1364 (2022).
3. J. A. Steens, J. van der Oost, R. H. J. Staals, *Mol. Cell* **82**, 4405–4406 (2022).
4. J. A. Steens *et al.*, *Nat. Commun.* **12**, 5033 (2021).
5. J. R. Elmore *et al.*, *Genes Dev.* **30**, 447–459 (2016).
6. M. A. Estrella, F. T. Kuo, S. Bailey, *Genes Dev.* **30**, 460–470 (2016).
7. M. Kazlauskiene, G. Tamulaitis, G. Kostiuk, Č. Venclovas, V. Siksnys, *Mol. Cell* **62**, 295–306 (2016).
8. O. Niewoehner *et al.*, *Nature* **548**, 543–548 (2017).
9. M. Kazlauskiene, G. Kostiuk, Č. Venclovas, G. Tamulaitis, V. Siksnys, *Science* **357**, 605–609 (2017).
10. B. Lowey *et al.*, *Cell* **182**, 38–49.e17 (2020).
11. K. S. Makarova, V. Anantharaman, N. V. Grishin, E. V. Koonin, L. Aravind, *Front. Genet.* **5**, 102 (2014).
12. K. S. Makarova *et al.*, *Nucleic Acids Res.* **48**, 8828–8847 (2020).
13. A. M. Burroughs, D. Zhang, D. E. Schäffer, L. M. Iyer, L. Aravind, *Nucleic Acids Res.* **43**, 10633–10654 (2015).
14. S. P. B. van Beljouw *et al.*, *Science* **373**, 1349–1353 (2021).
15. C. Rouillon *et al.*, *Nature* **614**, 168–174 (2023).

16. A. T. Whiteley *et al*., *Nature* **567**, 194–199 (2019).
17. D. Cohen *et al*., *Nature* **574**, 691–695 (2019).
18. S. Grüschow, C. S. Adamson, M. F. White, *Nucleic Acids Res.* **49**, 13122–13134 (2021).
19. L. M. Malone *et al*., *Nat. Microbiol.* **5**, 48–55 (2020).
20. L. Aravind, E. V. Koonin, *Proteins* **46**, 355–367 (2002).
21. K. McLuskey, J. C. Mottram, *Biochem. J.* **466**, 219–232 (2015).
22. Q. Shangguan, S. Graham, R. Sundaramoorthy, M. F. White, *Nucleic Acids Res.* **50**, 11214–11228 (2022).
23. R. K. Lau *et al*., *Mol. Cell* **77**, 723–733.e6 (2020).
24. H. T. Ichikawa *et al*., *PLOS ONE* **12**, e0176221 (2017).
25. G. Hogrel *et al*., *Nature* **608**, 808–812 (2022).
26. K. M. Boatright, G. S. Salvesen, *Curr. Opin. Cell Biol.* **15**, 725–731 (2003).
27. E. S. Alnemri *et al*., *Cell* **87**, 171 (1996).
28. R. V. Talanian *et al*., *J. Biol. Chem.* **272**, 9677–9682 (1997).
29. D. Carmona-Gutierrez, K. U. Fröhlich, G. Kroemer, F. Madeo, *Cell Death Differ.* **17**, 377–378 (2010).
30. S. J. Martin, in *Pathobiology of Human Disease: A Dynamic Encyclopedia of Disease Mechanisms*, L. M. McManus, R. N. Mitchell, Eds. (Elsevier, 2014).
31. N. Watanabe, E. Lam, *J. Biol. Chem.* **280**, 14691–14699 (2005).
32. D. Vercammen *et al*., *J. Biol. Chem.* **279**, 45329–45336 (2004).
33. T. J. Fan, L. H. Han, R. S. Cong, J. Liang, *Acta Biochim. Biophys. Sin.* **37**, 719–727 (2005).
34. J. Strecker *et al*., *Science* **378**, 874–881 (2022).
35. F. L. Gratani *et al*., *mSystems* **8**, e0104322 (2023).
36. F. Depardieu *et al*., *Cell Host Microbe* **20**, 471–481 (2016).

ACKNOWLEDGMENTS

We thank R. Fregoso Ocampo for assistance with negative-stain EM imaging. **Funding:** This work was funded by Dutch Research Council (NWO) VIDI grant VI.Vidi.203.074 (R.H.J.S.), NWO Spinoza grant SPI 93-537 (J.v.d.O.), European Research Council (ERC) Advanced grant ERC-AdG-834279 (J.v.d.O.), ERC CoG grant 817834 (T.J.G.E.), NWO VICI grant VI.C.192.016 (T.J.G.E.), Volkswagen Foundation grant 96725 (T.J.G.E.), National Institute of General Medical Sciences of the National Institutes of Health grant R35GM138348 (D.W.T.), Welch Foundation research grant F-1938 (D.W.T.), a Robert J. Kleberg, Jr. And Helen C. Kleberg Foundation medical research grant (D.W.T.), and American Cancer Society Research Scholar grant RSG-21-050-01-DMC (D.W.T.). **Author contributions:** Conceptualization and design: J.A.S., J.v.d.O., R.H.J.S.; Gene cluster and phylogenetic analyses: S.K., T.J.G.E.; Experiments and analyses: J.A.S., J.P.K.B., C.R.P.S., C.Y., A.M.A., S.H.P.P., A.S.A., C.P., A.Bard., A.Bare., R.A.S.; Writing: J.A.S., J.P.K.B., J.v.d.O., S.K., T.J.G.E., D.W.T., R.H.J.S. **Competing interests:** J.A.S. and S.H.P.P. are founders and shareholders of Scope Biosciences B.V., J.v.d.O. and R.H.J.S. are shareholders and members of the scientific board of Scope Biosciences B.V., and J.v.d.O. is a scientific advisor of NTrans Technologies and Hudson River Biotechnology. J.A.S., S.H.P.P., J.v.d.O., and R.H.J.S. are inventors on CRISPR-Cas related patents and patent applications. J.P.K.B., C.R.P.S., C.Y., A.M.A., S.K., A.S.A., C.P., A.Bard., A.Bare., R.A.S., T.J.G.E., and D.W.T. declare that they have no competing interests. **Data and materials availability:** All data are available in the manuscript. The raw mass spectrometry proteomics data have been deposited to the ProteomeXchange Consortium via the PRIDE partner repository with the dataset identifier PXD046897.

SUPPLEMENTARY MATERIALS

science.org/doi/10.1126/science.adk0378
Materials and Methods
Figs. S1 to S21
Tables S1 and S2
References (*37*–*42*)
MDAR Reproducibility Checklist

Submitted 2 August 2023; accepted 20 December 2023
10.1126/science.adk0378